Predicting response to breast cancer neoadjuvant chemotherapy using diffuse optical spectroscopy

Albert Cerussi*†, David Hsiang‡, Natasha Shah*, Rita Mehta‡, Amanda Durkin*, John Butler‡, and Bruce J. Tromberg*†

*Laser Medical and Microbeam Program, Beckman Laser Institute and Medical Clinic, University of California, 1002 Health Sciences Road East, Irvine, CA 92612; and ‡Chao Comprehensive Cancer Center, Division of Oncological Surgery, University of California Irvine Medical Center, 101 The City Drive, Orange, CA 92868

Communicated by Britton Chance, University of Pennsylvania School of Medicine, Philadelphia, PA, December 21, 2006 (received for review February 9, 2006)

Diffuse optical spectroscopy (DOS) and imaging are emerging diagnostic techniques that quantitatively measure the concentration of deoxy-hemoglobin (ctHHb), oxy-hemoglobin (ctO_2Hb), water (ctH_2O), and lipid in cm-thick tissues. In early-stage clinical studies, diffuse optical imaging and DOS have been used to characterize breast tumor biochemical composition and monitor therapeutic response in stage II/III neoadjuvant chemotherapy patients. We investigated whether DOS measurements obtained before and 1 week into a 3-month adriamycin/cytoxan neoadjuvant chemotherapy regimen can predict final, postsurgical pathological response. Baseline DOS measurements of 11 patients before therapy revealed significant increases in tumor ctHHb, ctO_2Hb, ctH_2O, and spectral scattering slope, and decreases in bulk lipids, relative to normal breast tissue. Tumor concentrations of ctHHb, ctO_2Hb, and ctH_2O dropped 27 ± 15%, 33 ± 7%, and 11 ± 15%, respectively, within 1 week (6.5 ± 1.4 days) of the first treatment for pathology-confirmed responders (n = 6), whereas nonresponders (n = 5) and normal side controls showed no significant changes in these parameters. The best single predictor of therapeutic response 1 week posttreatment was ctHHb (83% sensitivity, 100% specificity), while discrimination analysis based on combined ctHHb and ctH_2O changes classified responders vs. nonresponders with 100% sensitivity and specificity. In addition, the pretreatment tumor-to-normal ctO_2Hb ratio was significantly higher in responders (2.82 ± 0.44) vs. nonresponders (1.82 ± 0.49). These results highlight DOS sensitivity to tumor cellular metabolism and biochemical composition and demonstrate its potential for predicting and monitoring an individual's response to treatment.

diffuse optical imaging | frequency-domain photon migration | near-infrared | tissue spectroscopy | translational research

Optimal management locally advanced breast cancer (LABC) remains a complex therapeutic problem (1). LABC represents 5–20% of all newly diagnosed breast cancers in the United States with a higher incidence in medically underserved areas (2). Treatment for LABC has evolved from radical mastectomy to preoperative neoadjuvant chemotherapy followed by mastectomy or breast conservation therapy (3). Despite aggressive local therapy, long-term patient survival is still poor. LABC remains controversial because of uncertainties in determining the optimal intensity and duration of neoadjuvant chemotherapy and evaluating therapeutic response (2, 4, 5).

Neoadjuvant chemotherapy response is determined by serial physical examination, mammography and/or ultrasound. Complete pathological response (cPR) is an important therapeutic endpoint that is a surrogate for eradicating micrometastases, and strongly correlates with patient survival (6). Thus one goal of neoadjuvant chemotherapy monitoring is to determine early when a patient will demonstrate cPR. Many studies revealed significant discrepancies between clinical response assessments and final pathology (7–9).

A recent study (10) evaluating palpation, mammography, ultrasound, and MRI showed 19%, 26%, 35%, and 71% agreement, respectively, with pathological response. Functional measurements based on contrast-enhanced MRI (11), magnetic resonance spectroscopy (12, 13), and positron-emission tomography (14, 15) have shown substantial improvement over conventional anatomic assessment methods. However, these techniques can be difficult to perform in advanced-stage cancer patients because of lengthy scan times and the use of exogenous contrast, particularly if frequent measurements are desired.

Diffuse optical spectroscopy (DOS) is a noninvasive, bedside technique that quantitatively measures near-infrared (NIR) absorption and reduced scattering spectra. Absorption spectra determine the tissue concentration (ct) of oxygenated (ctO_2Hb) and deoxygenated hemoglobin (ctHHb), water (ctH_2O), and bulk lipid, the dominant NIR molecular absorbers in breast. DOS does not require exogenous contrast and rapidly (e.g., tens of seconds) provides quantitative, functional information about tumor biochemical composition, making it desirable from a patient perspective. Typically DOS samples a low number of spatial locations with a large spectral bandwidth. In contrast, diffuse optical imaging (DOI) typically samples a large number of spatial locations but with low spectral bandwidth. The relationship between DOS and DOI is comparable to that of magnetic resonance spectroscopy and MRI.

We recently reported the use of DOS to track tumor response to neoadjuvant chemotherapy in a human subject (16). DOS measurements were performed during neoadjuvant chemotherapy treatments, similar to the ones reported here. Changes in tissue biochemical composition were quantified over a three-cycle, 68-day adriamycin/cytoxan (A/C) regimen. Significant reductions in total tumor hemoglobin (ctTHb) and water content of 56% and 67%, respectively, were observed by the final treatment (17). Lipids increased by nearly 28%. Recent DOI studies supported these findings by coregistration with established imaging techniques after long-term treatment (18–20).

An important finding in Jakubowski *et al.* (16) was that significant changes in NIR optical properties occurred within a few days of the initial treatment. In this article, we report results from an expanded 11-patient study focused on correlations between tumor functional properties and final pathological response. Our goal is to provide quantitative functional information that could be used both before and during therapy to optimize individual patient response, evaluate novel dosing regimens, and assist the development of experimental therapeutics.

Results

Tumor Versus Normal Spectra. NIR spectra of breast tissues were acquired noninvasively with a handheld probe (Fig. 1) at discrete

Author contributions: A.C., D.H., and B.J.T. designed research; D.H., N.S., R.M., and A.D. performed research; A.C. and N.S. analyzed data; A.C. and B.J.T. wrote the paper; and D.H., R.M., and J.B. handled patient care.

Conflict of interest statement: One patent has been issued and another is pending for the DOS technology developed by A.C. and B.J.T. and described in this work.

Freely available online through the PNAS open access option.

Abbreviations: DOS, diffuse optical spectroscopy; NIR, near-infrared; DOI, diffuse optical imaging; A/C, adriamycin/cytoxan; THb, tumor hemoglobin; SP, scatter power.

†To whom correspondence may be addressed. E-mail: acerussi@uci.edu or bjtrombe@uci.edu.

www.pnas.org/cgi/doi/10.1073/pnas.0611058104

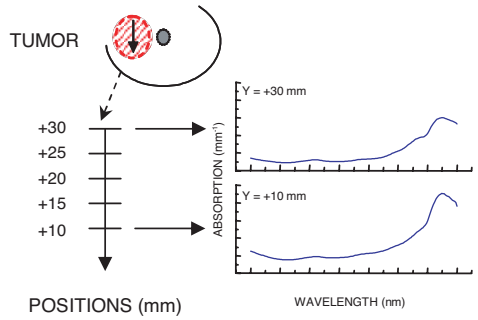

Fig. 1. Typical DOS measurement geometry, defining the optical linescan taken over a known tumor location. Complete NIR absorption and scattering spectra were measured at each location.

locations. Typical NIR diffuse optical spectra of normal and tumor tissues are provided in Fig. 2 from a 31-year-old surgically postmenopausal patient in this study with a 30-mm carcinoma. In Fig. 2 *Left*, the dots are the measured absorption spectrum and the solid lines are compositional fits using ctHHb, ctO_2Hb, ctH_2O, and lipids. In Fig. 2 *Right*, the dots are the discrete frequency-domain reduced scattering measurements, and the solid lines are the results of a power-law fit over the entire NIR spectrum. The measured tumor spectra correspond to a single linescan location over the tumor, whereas the normal spectra correspond to the same region on the contralateral normal breast. The error bars are plotted every 50 nm for clarity and represent the standard deviation of two independent linescan measurements.

NIR spectra demonstrate distinct differences between tumor and normal tissues. Below 850 nm, tumor absorption is increased relative to normal due to ctHHb and ctH_2O increases. At wavelengths in the vicinity of 980 nm, where there is a water absorption peak from O—H vibrational overtones, the heightened tumor absorption is also evident. The peak in the normal absorption spectrum at 930 nm is representative of vibrational overtones of

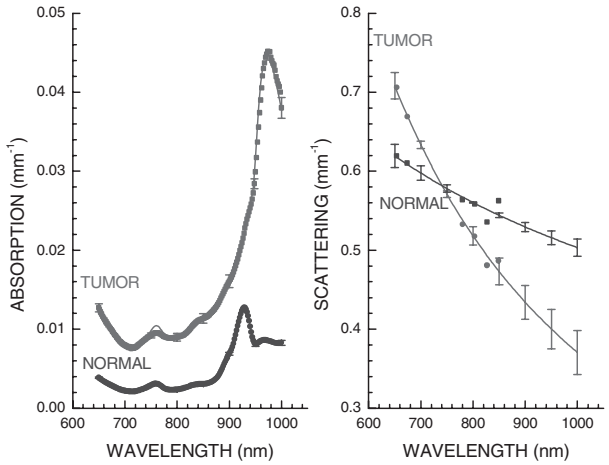

Fig. 2. NIR absorption (*Left*) and reduced scattering (*Right*) spectra obtained noninvasively from a 30-mm diameter tumor in the breast of a neoadjuvant chemotherapy subject. (*Left*) The heightened absorption results from a combination of increased hemoglobin and water relative to normal breast tissue. (*Right*) The sharp spectral decrease in scattering for tumor tissue is likely due to increases in both cellular density and fibrous tissue in tumor tissue relative to normal breast tissue. Tumor spectra were obtained from the +10-mm position, whereas the normal spectra were taken from the corresponding contralateral position on the normal side. Error bars are the variation from two independent linescans (plotted every 50 nm for clarity).

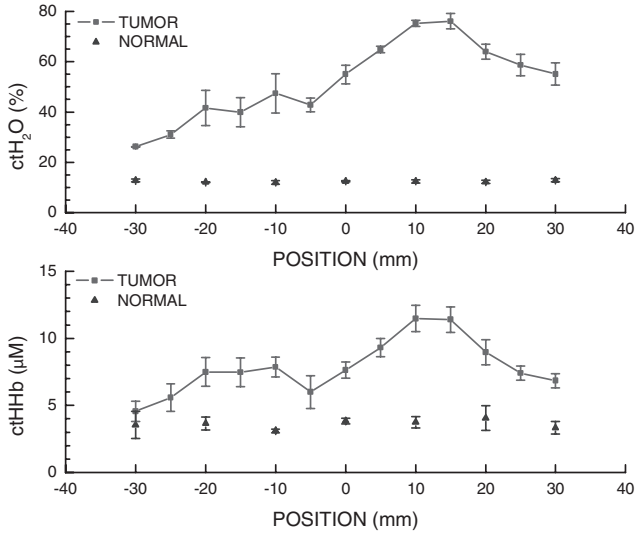

Fig. 3. Linescan results of ctH_2O (*Upper*) and ctHHb (*Lower*) from the same patient as in Fig. 2. NIR spectra at each linescan location are used to calculate NIR absorber concentrations at each spatial location. Error bars are the variations between two independent linescans.

lipid C—H bonds. This prominent lipid peak is typically reduced in tumor tissues (21).

The wavelength-dependent tissue scattering (i.e., the scatter power, SP) also differs substantially between tumor and normal tissues. The tumor-scattering spectrum in Fig. 2 *Right* decays more rapidly than in normal tissue, suggesting alterations in scattering center density and size (21–23). Similar effects have been observed for *in vitro* light scattering studies of malignant cell suspensions, although *in vivo* the extracellular matrix also contributes to scattering (21, 22).

The spatial variations of both ctH_2O and ctHHb are demonstrated in Fig. 3 on the same patient as Fig. 2. Error bars represent the standard deviation of two independent linescans. The concentrations of tissue chromophores are calculated from the absorption spectrum measured at each linescan location (i.e., Fig. 2). The general spectral features revealed in Fig. 2 predict large ctH_2O and ctHHb increases in tumor relative to contralateral normal tissues. The physiological perturbation of the tumor, centered at +10 mm, extends beyond the +30 mm spatial extent of the lesion itself. The perturbation in tissue physiology caused by this tumor is far greater than both normal tissue physiological variation or measurement errors.

General Tumor Functional Properties. The optically measured functional characteristics of all 11 tumors before treatment are summarized in Table 1. The first is the average value of the DOS-parameter on the contralateral normal side (normal), which was assumed to be normal tissue unless otherwise suggested in clinical and radiological reports (i.e., the average of all normal linescan points in Fig. 3). The second value in Table 1 is the peak value of

Table 1. Baseline tumor functional properties

Parameter	Normal	Tumor max	*Z*
ctHHb, μM	4.57 ± 1.35	10.6 ± 3.81	0.0003*
ctO_2Hb, μM	9.05 ± 4.14	19.5 ± 12.7	0.007*
ctH_2O, %	13.9 ± 4.61	41.2 ± 25.1	0.001*
Lipid, %	65.1 ± 9.67	40.0 ± 18.4	0.0025*
SP	0.54 ± 0.18	0.95 ± 0.42	0.013*

*, Significant result.

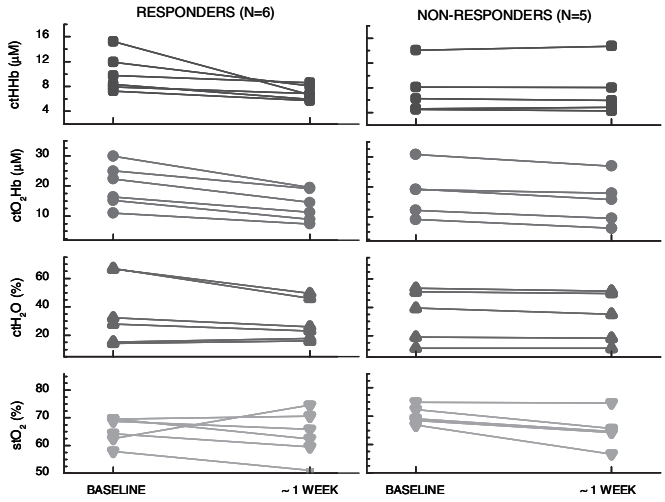

Fig. 4. Plots of changes in tumor ctHHb, ctO_2Hb, ctH_2O, and stO_2 for individual patients, stratified by final pathological response. The plotted value is the average of the DOS parameter within the FWHM. The baseline and ~1 week points correspond to the measurements taken within 1 week before and within 1 week after the start of therapy, respectively. Responder changes are distinctive from nonresponders. Error bars for the individual measurements are not presented for clarity (5–10%).

the tumor linescan (tumor max), which was assumed to be the best representative location of the tumor (i.e., the +10-mm tumor linescan location in Fig. 3). The Z value is the result of a two-tailed nonparametric Wilcoxon rank sums test, where significance was assumed to be 0.05. Error bars represent the standard deviation of the population (i.e., not the standard error).

We found that tumor max was significantly different from normal, as expected. Tumor/normal differences were found to be significant for all DOS-measured parameters. These trends were confirmed in a more detailed analysis of 58 patients (21). Similar results have been observed in clinical studies with discrete wavelength instruments that are primarily sensitive to hemoglobin (24–28).

In general, no statistically significant differences between baseline optical properties were found between responder and nonresponder groups. However, we did observe that the ratio of tumor-to-normal (T/N) ctO_2Hb was significantly higher ($Z = 0.023$) in the responder group (T/N = 2.82 ± 0.44) than in the nonresponder group (T/N = 1.82 ± 0.49).

Sensitivity to Chemotherapy: Binary Classification. Fig. 4 shows the changes resulting from neoadjuvant chemotherapy measured in ctHHb, ctO_2Hb, ctH_2O, and tissue hemoglobin saturation (stO_2 = ctO_2Hb/ctTHb) for each subject, stratified by a binary pathological response classification of responder vs. nonresponder (see *Materials and Methods*). Each line represents one patient, where the two points correspond to DOS measurements taken within a week before and within a week after neoadjuvant chemotherapy. The points are the value of a DOS parameter averaged over the tumor region, which was several linescan points. ctO_2Hb drops from baseline in all patients, whereas ctHHb drops only in all responder patients. ctH_2O for the most part decreases for responders and remains constant for nonresponders. stO_2 generally decreases for all patients. Error bars are not shown for clarity, but are comparable to those in Fig. 3 (≈5–10%).

Table 2 summarizes neoadjuvant chemotherapy effects on all five measured base parameters, averaged by response category. The best predictor of therapeutic response was ctHHb. The average ctHHb relative value drop was 27% (0.73 ± 0.17) in responders, which was significantly different from nonresponders (1.02 ± 0.05)

Table 2. Normalized postchemotherapy changes

Parameter	Responder	Nonresponder	Z
ctHHb, μM	0.73 ± 0.17	1.02 ± 0.05	0.008*
ctO_2Hb, μM	0.67 ± 0.06	0.82 ± 0.10	0.03*
ctH_2O, %	0.89 ± 0.2	0.96 ± 0.03	0.41
ctH_2O, relative	0.80 ± 0.08	0.96 ± 0.03	0.008*
Lipid, %	1.30 ± 0.3	1.11 ± 0.14	0.41
SP	0.88 ± 0.20	0.97 ± 0.20	0.93

*, Significant result.

($Z = 0.008$, two-tailed, 95% confidence). ctO_2Hb also decreased significantly after therapy ($Z = 0.02$). Unlike ctHHb, both groups dropped in ctO_2Hb: nonresponders by 18% (0.82 ± 0.10) and responders by 33% (0.67 ± 0.06). These findings suggest that chemotherapy-induced alterations in ctHHb may be a more sensitive index of cellular oxygen consumption and local metabolism. In contrast, ctO_2Hb levels are likely to be more reflective of global vascular effects (16). Thus, the additional 25% drop in ctO_2Hb for responders (i.e., from 18% to 33%) is likely caused by therapy-induced changes to tumor microvasculature.

ctH_2O also changed in response to neoadjuvant chemotherapy. For the nonresponder group, ctH_2O values remained nearly constant (0.96 ± 0.03), whereas for the responder group, ctH_2O decreased (0.89 ± 0.2). The difference between these changes was not statistically significant ($Z = 0.4$). In some cases, ctH_2O increased after therapy [an effect previously seen (16)], and in other cases ctH_2O arrived at a peak value a few days after therapy only to decrease below baseline 1 week later. If we consider the absolute value of the change from baseline, we then discover that relative ctH_2O changes (20%) are significant ($Z = 0.008$). The dynamics of this ctH_2O increase and subsequent decrease is likely caused by individual variations in tumor drug response, edema, and necrosis.

Both SP and lipids changed after therapy, but not in statistically significant fashion ($Z = 0.93$ and 0.41, respectively). Lipid changes were the most volatile, increasing slightly in both cases. We observed a slightly higher increase in lipids in the responder population than in the nonresponder population, but the difference was not statistically significant. Similarly, we observed a decrease in SP in responders relative to nonresponders.

Observed changes in the tumors of responders cannot be accounted for by measurement errors, menstrual cycle variations, or other physiological variations. Each patient served as her own control using measurements from the contralateral normal side. For responders, changes in tumor ctHHb, ctO_2Hb, and ctH_2O were significantly different from fluctuations measured in contralateral normal breast tissues for each patient. Normal variations generally affect the entire linescan, and thus preserve the absolute change of tumor values relative to the baseline. In addition, the greatest changes were always in the breast region identified as the tumor. On average, across the population changes in tumor ctHHb, ctO_2Hb, and ctH_2O were significant relative to changes in normal tissues ($Z = 0.008$, 0.008, and 0.011, respectively). In addition, measurements of ctTHb decreased in all six responder subjects (Fig. 4).

Predicting Pathological Response. Table 3 displays the results of discrimination analysis using DOS-measured parameters as the predictors, assuming an equal probability for response and nonresponse. Calculations of sensitivity and specificity were determined by the success of the discriminant function to predict the known final pathological response. The results of a single-parameter analysis show that ctHHb is the best response predictor, followed by relative changes in ctH_2O. One patient of 11 was misclassified when using only ctHHb as a predictor. ctO_2Hb also performed well in this limited sample. Parameters that report more on tissue structure

Table 3. Results of discrimination analysis (binary classification)

Parameter	Sensitivity, %	Specificity, %
ctHHb	83	100
ctO_2Hb	83	80
ctH_2O	67	80
ctH_2O, relative	80	100
Lipid	50	80
SP	50	80
stO_2	50	80
ctTHb	100	100
ctHHb and ctH_2O, relative	100	100

(i.e., lipids and SP) were not good single predictors, because more time is needed before tumor size changes are detectable.

If we use a second parameter in the discrimination analysis (e.g., relative water changes and ctHHb), we find that perfect classification can be achieved (i.e., 100% sensitivity and 100% specificity). Results will naturally improve by combining strong predictors. However, not all combinations of basis components were successful. For example, two commonly used hemodynamic indices, ctTHb (= ctHHb+ctO_2Hb) and stO_2 (= ctO_2Hb/ctTHb×100%) yielded mixed results. As single predictors, ctTHb yielded 100% sensitivity and 100% specificity whereas stO_2 was inadequate. stO_2 has received much attention because it is based on relative values, yet our analysis suggests that stO_2 alone is not a good predictor of pathological response. Because it appears that ctHHb and ctH_2O are independent of systemic chemotherapy effects, the combination of ctHHb and ctH_2O may in general serve as a better indicator of response than ctHHb and ctO_2Hb.

Discussion

Medical diagnostic techniques based on NIR transillumination were first introduced in the 1920s to detect breast cancer (29). Although NIR light penetrates tissue to depths of several centimeters, early methods were not successful because these approaches were qualitative and did not account for distortions from multiple light scattering. Current DOI and DOS technologies make it possible to separate light absorption from scattering and quantify subtle changes in biochemical composition in thick tissues. While the spatial resolution of DOS is inferior to conventional anatomic imaging methods, patients undergoing neoadjuvant chemotherapy have large, well localized tumors (e.g., ≈2–10 cm). Consequently, their position is known *a priori*, and DOS measurements can be optimized for sensitivity to tumor functional changes rather than size or volumetric changes that may occur later in the treatment (30).

Previous work suggests that early tumor biochemical alterations are predictive of pathological response. Significant biochemical changes were observed within 24 h posttherapy in a murine mammary adenocarcinoma model using ^{31}P-magnetic resonance spectroscopy (31). Increases in apoptosis resulting from chemotherapy have been observed in solid tumors via biopsy within 24 h posttherapy (32). Although dynamics vary, apoptotic activity peaks within 4 days posttreatment, as measured by serial fine needle aspiration (33). Apoptotic activity 24 h posttherapy is not necessarily a good predictor of final pathological response or survival (34). A similar trend has been observed for diminished proliferation, as measured by Ki67 immunohistochemical assays (32–34). However, a combination of apoptosis and proliferation markers, termed the growth index, appears to be an excellent predictor of response (34).

Anthracycline derivatives, such as the doxorubicin used in this trial, have been found to induce both an early increase in apoptotic activity and a decrease in proliferation (35). We expect that cellular assays will correlate with DOS functional measurements of biochemical changes within 1 week posttherapy. The nature of these response dynamics may require daily monitoring early in the treatment cycle, as evidenced by Archer *et al.* (34) and our own observations of water fluctuations.

A key question is whether early apoptotic and proliferative changes produce macroscopically detectable light-scattering signals that are predictive of pathological response. DOS, which relies solely on endogenous contrast in this study, does not directly measure proliferation or apoptosis. However, DOS-measured tissue hemoglobin (36) is representative of tumor microvasculature (37), which is sensitive to cellular metabolism.

The overall decrease in ctTHb is a consequence of alterations in tumor cell metabolism, blood vessel density, and systemic effects. These processes can be separated, in part, by considering ctO_2Hb and ctHHb independently. The ctO_2Hb decrease can be attributed primarily to vascular supply, while ctHHb is representative of tumor tissue oxygen consumption. As tumor cells undergo apoptosis and reduce proliferation, oxygen delivery and consumption diminish. DOS is sensitive to these events, as indicated by the drop in ctO_2Hb and ctHHb levels, respectively. With increased cell death, the loss of oxygen consuming sources (i.e., cells) causes tumor ctHHb levels to drop even further. Although we have provided endogenous measurements of tumor ctTHb, additional information about tumor hemodynamics (i.e., flow) could be helpful for assessing therapeutic response. This is especially important because a more complete metabolic picture can be formed from ctHHb, ctO_2Hb, and flow (38, 39).

The role of microvascular changes in chemotherapeutic response prediction has provided mixed results. Small decreases in tumor microvessel density (MVD) have been observed when comparing pretreatment (i.e., baseline) to presurgery. However, these results failed to demonstrate significant differences between responders based on MVD (40). Positron-emission tomography studies have shown that tumor blood blow changes 2 months posttherapy relative to baseline are predictive of patient response to chemotherapy and patient survival (15). Other studies have shown that systemic total hemoglobin levels correlate with response (41). Perhaps more important is the hemoglobin available to the tumor, which DOS measures directly.

Tumor ctH_2O also has important biochemical significance that has not been used in optical studies of tumors. Insight into ctH_2O can be derived from MRI studies of the apparent diffusion coefficient of water (ADC_w). The ADC_w correlates with cellular density in several tissues, including brain (42–44), breast (45–47), and bone marrow (48). Detailed studies using human melanoma xenografts (49) and breast tumor animal models (50) have supported these findings. The ADC_w also relates to cellular pathology (48, 51). Optically detected changes in ctH_2O may represent subtle variations in tumor cell density and edema, where reductions in tumor water imply diminished cellularity due to cell death (52). Recent studies in murine tumor models support this concept and suggest that changes in the ADC_w reflect tumor therapeutic response (53).

Although our study suggests that early changes in NIR-measured tumor physiology can predict final pathological response, predicting pathological response before therapy is equally challenging and desirable. To explore this possibility, we compared pretreatment DOS parameters for responders and nonresponders. Significantly higher tumor-to-normal ctO_2Hb ratios were found in the responder population ($Z = 0.023$). This elevated ratio reflects increased tumor blood supply and oxygen availability, factors that are likely to improve drug delivery and utilization. Our preliminary observation obtained using noninvasive technology supports previous research that tumor blood flow, oxygenation, and metabolism can significantly influence therapeutic efficacy (54).

The overall discrimination analysis results are encouraging but preliminary. It is not surprising that ctHHb is the best single predictor of response. Parameters that report primarily on tissue matrix (bulk lipid and SP) were not strong predictors of pathological

response because within 1 week of therapy, gross tumor size changes are typically not observed. Generally, any parameter combined with ctHHb yielded perfect or near-perfect classification results. However, the use of ctO_2Hb yielded perfect classification only when used in combination with ctHHb. It is tempting to further stratify final pathological response (i.e., complete pathological response, partial pathological response, nonpathological response), but this is not possible with our population distribution. It is possible that additional clinical information (i.e., pretherapy biopsies) may be important for improving results in a significantly larger patient population. We suspect that a more detailed analysis of the ctHHb, ctO_2Hb, and ctH_2O kinetics within the early stages of therapy may help stratify final pathological response.

Conclusion

Endogenous *in vivo* optical biomarkers can predict pathological response in treated tumors. Although these parameters lack the specificity of conventional gene or protein-based biomarkers, DOS measurements of biochemical composition report "downstream" tissue vascular and cellular physiology. These quantitative functional endpoints have practical clinical potential to predict therapeutic outcome and minimize patient toxicity. In addition, DOS and DOI can be used as translational research tools in humans and preclinical animal models to facilitate drug discovery and develop individualized therapeutic dosing strategies.

Materials and Methods

Instrument Design. The concepts of our combined frequency-domain (55) and continuous-wave (56) tissue spectrometer system and the specific details of the instrument have been reported (16). The frequency-domain component of the instrument allowed for absolute quantification of tissue optical properties at discrete wavelengths, while the continuous wave component determined the optical properties at continuous wavelengths across the NIR (650–1,000 nm) spectrum. The frequency-domain portion of the DOS instrument used six commercially available diode laser sources (660, 690, 780, 808, 830, and 850 nm) and an avalanche photodiode (APD) detector. The steady-state portion of the DOS instrument used a fiber-coupled broadband white-light source and a fiber-coupled 16-bit, 1,024-pixel, cooled CCD spectrometer. The spectrometer system detected broadband light from 650 to 1,000 nm with 8-nm spectral resolution. A handheld probe incorporated all source optical fibers and the APD and spectrometer detector fiber. A reflectance geometry with a 28-mm source detector separation was used. Measurements were performed by using a timing technique with 20 mW of optical power incident to the tissue per source. Frequency-domain instrumental artifacts were removed by calibrating with a tissue-simulating phantom with known absorption and scattering properties. Spectral artifacts were removed by calibrating on a spectraflect-coated integrating sphere.

Measurement linescans were generated by moving the probe to a set of discrete positions in either 5- or 10-mm steps (Fig. 1). Tumor locations were known *a priori* from mammography, ultrasound, and palpation. Full absorption and reduced scattering spectra were measured at each grid location, as indicated in Fig. 1. A complete measurement of tissue absorption and scattering spectra required 30–45 s at each linescan location. Linescans were repeated twice at each location to evaluate placement errors. The fraction of tumor to normal tissue sampled by the light depended on the tissue optical properties and the lesion depth. The region of maximum contrast (tumor maximum) was assumed to be the best representation of the tumor.

Measured Information. Calculations using the Beer-Lambert law and known absorber extinction coefficients were used to convert the absorption spectra (Fig. 2 *Left*) into the tissue concentrations of ctHHb (μM), ctO_2Hb (μM), ctH_2O (%), and bulk lipids (%), which are the primary NIR absorbers in breast tissue (57). ctH_2O is the concentration of measured tissue water divided by pure water concentration (55.6 M). Tissue bulk lipids are reported as relative to an assumed "pure" lipid density of 0.9 g·ml^{-1}. Reported water and bulk lipid percentages are relative figures of merit compared with pure solutions of the substance and are neither strict volumes nor add up to 100%. Tissue reduced scattering properties are reported as the results of a power-law fit to the measured frequency-domain reduced scattering (22). The absolute value of the exponent from this fit is termed the SP. The SP is related to the size of the tissue scattering particles in relation to the optical wavelength.

Patient Characteristics. Eleven cancer patients receiving neoadjuvant chemotherapy were studied. All subjects provided informed written consent according to an institution-approved protocol (University of California Irvine 02-2306). The average subject age was 47.4 ± 11.4 years with a range of 30 to 65, and the average body mass index was 28.8 ± 5.6 with a range of 21.6 to 41.2. Before treatment, the average tumor maximum-length axis was 37 ± 23 mm, with a median of 30 mm, and a range of 18 to 95 mm. Two subjects were premenopausal, and the remaining nine were postmenopausal.

Final pathological response was determined from standard pathology. Initial lesion sizes were determined by ultrasound. Pathological response was stratified into a binary classification scheme of responders ($n = 6$) and nonresponders ($n = 5$). Consistent with radiological definitions, responders were defined as subjects with >50% change in the maximum-tumor axis in final pathology dimensions relative to the initial maximum axis dimension. The remaining subjects were considered to be nonresponders. Although pathological and radiological tumor sizes may not agree, the general trends are preserved.

Under a tertiary classification scheme (58), the breakdown was: complete pathological response ($n = 1$), partial pathological response ($n = 8$), and nonpathological response ($n = 2$). Tertiary/quaternary response scales present a more realistic gradation scale for pathological assessment, although these scales are still far from quantitative. It is desirous to represent these more realistic gradation scales, but low patient numbers do not permit a proper statistical analysis.

Chemotherapy Treatment Sequence. Nine of the 11 patients were treated with three to four cycles of A/C therapy, followed by three to four cycles of taxanes. The remaining 2 subjects received three cycles of A/C therapy without the taxanes. Each chemotherapy cycle lasted 3 weeks. Two additional measured subjects who received this treatment regimen were excluded from this prospective analysis. One subject did not complete the DOS measurements because of illness. The other subject responded poorly to the A/C regimen and was switched to another therapy. All treatment decisions were made using conventional means by the patient's physician.

Measurement Sequence. Linescans were performed within 1 week before and 1 week after the initial A/C treatment (Fig. 1). Initial DOS measurements were performed 2–4 weeks postbiopsy. At each location, broadband optical absorption and reduced scattering spectra were obtained (Fig. 2). On average, measurements were performed 1.8 ± 4.5 days before and 6.5 ± 1.4 after the initial A/C therapy. Baseline measurements were performed within 1 week of therapy. The second date was chosen because most patients had DOS measurements near 1 week posttherapy due to scheduling considerations. For all 11 subjects, an average of 10 ± 2 points per DOS linescan were measured. The linescan length was proportional to lesion size. Linescans were geometrically much larger than the tumor dimensions and provided regions of normal breast tissue in the tumor vicinity. We took the points within the FWHM of the

linescan peak as the locations that best identified the tumor (6 ± 2 points per tumor, on average). DOS parameters within the FWHM were averaged to give a tumor value (i.e., Fig. 4). For the purposes of statistical comparisons (Tables 2 and 3), the tumor value was defined as the integral of the DOS parameter over the FWHM. We removed intersubject variations by analyzing the ratio of pretherapy and posttherapy tumor measurements; thus no change has the value of unity. Measurements were also performed on the contralateral normal breast to serve as a measure of normal physiological variations, although the effects of chemotherapy are not localized. Thus, patients served as their own controls.

Statistical Considerations. Comparisons between the two responder groups were performed by using nonparametric Wilcoxon rank sums or Kruskal-Wallis tests for two and three group comparisons, respectively. Significance was assumed at a confidence interval of 95% ($\alpha = 0.05$) for a two-tailed distribution in the Wilcoxon rank sums tests. We further assumed that all measurements were independent. All statistical calculations were performed with commercial software (JMP IN; SAS Institute, Cary, NC). Error bars for population data were the population standard deviation.

Discrimination analysis was also used to distinguish the two response groups based on the DOS measurements. The discrimination algorithm calculated a threshold score based on predictor values. We considered the DOS basis set (ctHHb, ctO_2Hb, ctH_2O, lipid, SP) as predictors. Normality violations for each basis parameter considered were not found to be significant with the Shapiro-Wilk test. We considered predictors that were simple functions of the base DOS parameters to retain physiological meaning. Only single- and dual-predictor variables were used because there were only two classification groups.

We thank Montana Compton, Tran Du, and the women who participated in this study. This work was supported by National Institutes of Health Grants P41-RR01192 (Laser Microbeam and Medical Program) and U54-CA105480 (Network for Translational Research in Optical Imaging), the California Breast Cancer Research Program, the Beckman Foundation, and Chao Family Comprehensive Cancer Center Grant P30-CA62203.

1. Carlson RW, Favret AM (1999) *Breast J* 5:303–307.
2. Mankoff DA, Dunnwald LK, Gralow JR, Ellis GK, Drucker MJ, Livingston RB (1999) *Cancer* 85:2410–2423.
3. Esteva FJ, Hortobagyi GN (1999) *Hematol Oncol Clin North Am* 13:457–472, vii.
4. Hortobagyi GN (1990) *Cancer* 66:1387–1391.
5. De Lena M, Varini M, Zucali R, Rovini D, Viganotti G, Valagussa P, Veronesi U, Bonadonna G (1981) *Cancer Clin Trials* 4:229–236.
6. Fisher B, Bryant J, Wolmark N, Mamounas E, Brown A, Fisher ER, Wickerham DL, Begovic M, DeCillis A, Robidoux A, *et al.* (1998) *J Clin Oncol* 16:2672–2685.
7. Feldman LD, Hortobagyi GN, Buzdar AU, Ames FC, Blumenschein GR (1986) *Cancer Res* 46:2578–2581.
8. Helvie MA, Joynt LK, Cody RL, Pierce LJ, Adler DD, Merajver SD (1996) *Radiology* 198:327–332.
9. Vinnicombe SJ, MacVicar AD, Guy RL, Sloane JP, Powles TJ, Knee G, Husband JE (1996) *Radiology* 198:333–340.
10. Yeh E, Slanetz P, Kopans DB, Rafferty E, Georgian-Smith D, Moy L, Halpern E, Moore R, Kuter I, Taghian A (2005) *AJR Am J Roentgenol* 184:868–877.
11. Warren RM, Bobrow LG, Earl HM, Britton PD, Gopalan D, Purushotham AD, Wishart GC, Benson JR, Hollingworth W (2004) *Br J Cancer* 90:1349–1360.
12. Chenevert TL, Stegman LD, Taylor JM, Robertson PL, Greenberg HS, Rehemtulla A, Ross BD (2000) *J Natl Cancer Inst* 92:2029–2036.
13. Meisamy S, Bolan PJ, Baker EH, Bliss RL, Gulbahce E, Everson LI, Nelson MT, Emory TH, Tuttle TM, Yee D, *et al.* (2004) *Radiology* 233:424–431.
14. Kim SJ, Kim SK, Lee ES, Ro J, Kang S (2004) *Ann Oncol* 15:1352–1357.
15. Mankoff DA, Dunnwald LK, Gralow JR, Ellis GK, Schubert EK, Tseng J, Lawton TJ, Linden HM, Livingston RB (2003) *J Nucl Med* 44:1806–1814.
16. Jakubowski DB, Cerussi AE, Bevilacqua F, Shah N, Hsiang D, Butler J, Tromberg BJ (2004) *J Biomed Opt* 9:230–238.
17. Makris A, Powles TJ, Kakolyris S, Dowsett M, Ashley SE, Harris AL (1999) *Cancer* 85:1996–2000.
18. Zhu Q, Kurtzma SH, Hegde P, Tannenbaum S, Kane M, Huang M, Chen NG, Jagjivan B, Zarfos K (2005) *Neoplasia* 7:263–270.
19. Shah N, Gibbs J, Wolverton D, Cerussi A, Hylton N, Tromberg BJ (2005) *J Biomed Opt* 10:51503.
20. Choe R, Corlu A, Lee K, Durduran T, Konecky SD, Grosicka-Koptyra M, Arridge SR, Czerniecki BJ, Fraker DL, DeMichele A, *et al.* (2005) *Med Phys* 32:1128–1139.
21. Cerussi A, Shah N, Hsiang D, Durkin A, Butler J, Tromberg BJ (2006) *J Biomed Opt* 11:044005.
22. Mourant JR, Fuselier T, Boyer J, Johnson TM, Bigio IJ (1997) *Appl Opt* 36:949–957.
23. Nilsson AMK, Sturesson C, Liu DL, Andersson-Engels S (1998) *Appl Opt* 37:1256–1267.
24. Taroni P, Danesini G, Torricelli A, Pifferi A, Spinelli L, Cubeddu R (2004) *J Biomed Opt* 9:464–473.
25. Grosenick D, Wabnitz H, Moesta KT, Mucke J, Schlag PM, Rinneberg H (2005) *Phys Med Biol* 50:2451–2468.
26. Chance B, Nioka S, Zhang J, Conant EF, Hwang E, Briest S, Orel SG, Schnall MD, Czerniecki BJ (2005) *Acad Radiol* 12:925–933.
27. Intes X (2005) *Acad Radiol* 12:934–947.
28. Zhu Q, Cronin EB, Currier AA, Vine HS, Huang M, Chen N, Xu C (2005) *Radiology* 237:57–66.
29. Cutler M (1929) *Surg Gynecol Obstet* 48:721–728.
30. Srinivasan S, Pogue BW, Dehghani H, Jiang S, Song X, Paulsen KD (2004) *J Biomed Opt* 9:1161–1171.
31. Evelhoch JL, Keller NA, Corbett TH (1987) *Cancer Res* 47:3396–3401.
32. Ellis PA, Smith IE, McCarthy K, Detre S, Salter J, Dowsett M (1997) *Lancet* 349:849.
33. Symmans WF, Volm MD, Shapiro RL, Perkins AB, Kim AY, Demaria S, Yee HT, McMullen H, Oratz R, Klein P, *et al.* (2000) *Clin Cancer Res* 6:4610–4617.
34. Archer CD, Parton M, Smith IE, Ellis PA, Salter J, Ashley S, Gui G, Sacks N, Ebbs SR, Allum W, *et al.* (2003) *Br J Cancer* 89:1035–1041.
35. Arpino G, Ciocca DR, Weiss H, Allred DC, Daguerre P, Vargas-Roig L, Leuzzi M, Gago F, Elledge R, Mohsin SK (2005) *Breast Cancer Res Treat* 92:69–75.
36. Pogue BW, Poplack SP, McBride TO, Wells WA, Osterman KS, Osterberg UL, Paulsen KD (2001) *Radiology* 218:261–266.
37. Liu H, Chance B, Hielscher AH, Jacques SL, Tittel FK (1995) *Med Phys* 22:1209–1217.
38. Durduran T, Choe R, Yu G, Zhou C, Tchou JC, Czerniecki BJ, Yodh AG (2005) *Opt Lett* 30:2915–2917.
39. Intes X, Ripoll J, Chen Y, Nioka S, Yodh AG, Chance B (2003) *Med Phys* 30:1039–1047.
40. Bottini A, Berruti A, Bersiga A, Brizzi MP, Allevi G, Bolsi G, Aguggini S, Brunelli A, Betri E, Generali D, *et al.* (2002) *Clin Cancer Res* 8:1816–1821.
41. Bottini A, Berruti A, Brizzi MP, Bersiga A, Generali D, Allevi G, Aguggini S, Bolsi G, Bonardi S, Bertoli G, *et al.* (2003) *Br J Cancer* 89:977–982.
42. Sugahara T, Korogi Y, Kochi M, Ikushima I, Shigematu Y, Hirai T, Okuda T, Liang L, Ge Y, Komohara Y, *et al.* (1999) *J Magn Reson Imaging* 9:53–60.
43. Filippi CG, Edgar MA, Ulug AM, Prowda JC, Heier LA, Zimmerman RD (2001) *AJNR Am J Neuroradiol* 22:65–72.
44. Kono K, Inoue Y, Nakayama K, Shakudo M, Morino M, Ohata K, Wakasa K, Yamada R (2001) *AJNR Am J Neuroradiol* 22:1081–1088.
45. Guo Y, Cai YQ, Cai ZL, Gao YG, An NY, Ma L, Mahankali S, Gao JH (2002) *J Magn Reson Imaging* 16:172–178.
46. Sinha S, Lucas-Quesada FA, Sinha U, DeBruhl N, Bassett LW (2002) *J Magn Reson Imaging* 15:693–704.
47. Thomas MA, Wyckoff N, Yue K, Binesh N, Banakar S, Chung HK, Sayre J, DeBruhl N (2005) *Technol Cancer Res Treat* 4:99–106.
48. Baur A, Dietrich O, Reiser M (2003) *Eur Radiol* 13:1699–1708.
49. Lyng H, Haraldseth O, Rofstad EK (2000) *Magn Reson Med* 43:828–836.
50. Paran Y, Bendel P, Margalit R, Degani H (2004) *NMR Biomed* 17:170–180.
51. Rowley HA, Grant PE, Roberts TP (1999) *Neuroimaging Clin N Am* 9:343–361.
52. Brauer M (2003) *Prog Neuropsychopharmacol Biol Psychiatry* 27:323–331.
53. Zhao M, Pipe JG, Bonnett J, Evelhoch JL (1996) *Br J Cancer* 73:61–64.
54. Vaupel P (1992) *NMR Biomed* 5:220–225.
55. Pham TH, Coquoz O, Fishkin JB, Anderson E, Tromberg BJ (2000) *Rev Sci Instrum* 71:2500–2513.
56. Bevilacqua F, Berger AJ, Cerussi AE, Jakubowski D, Tromberg BJ (2000) *Appl Opt* 39:6498–6507.
57. Cerussi AE, Jakubowski D, Shah N, Bevilacqua F, Lanning R, Berger AJ, Hsiang D, Butler J, Holcombe RF, Tromberg BJ (2002) *J Biomed Opt* 7:60–71.
58. Therasse P, Arbuck SG, Eisenhauer EA, Wanders J, Kaplan RS, Rubinstein L, Verweij J, Van Glabbeke M, van Oosterom AT, Christian MC, *et al.* (2000) *J Natl Cancer Inst* 92:205–216.